ChemPubSoc Europe

DOI: 10.1002/cctc.201901872

CHEMCATCHEM Full Papers

Tailoring the Photoelectrochemical Activity of TiO_2 Electrodes by Multilayer Screen-Printing

Carsten Günnemann,*[a] Mariano Curti,*[a] J. Gerrit Eckert,[a] Jenny Schneider,[b] and Detlef W. Bahnemann[a, c]

Screen-printing is a commonly used method for the preparation of photoelectrodes. Although previous studies have explored the effect of the number of printed layers on the efficiency of dye-sensitized solar cells, its interplay with the photoelectrocatalytic properties of the electrodes has rarely been examined. This study focuses on this issue by studying the photoelectrocatalytic oxidation of methanol over TiO_2 electrodes. Incident photon-to-current efficiencies reached 87% at the optimal conditions of monochromatic (338 nm) irradiation of one-layer films at 0.2 V vs NHE. However, the irradiation wavelength and applied bias strongly influenced the relative behavior of the films. For instance, at 0.5 V and 327 nm irradiation, the one-layer electrode was 6 times more efficient than the four-layer one, while at 385 nm the four-layer electrode was 3.5 times more efficient. The results were explained on the basis of differing light absorption properties and charge carrier lifetimes. Modelling and quantification of the electron diffusion length (5.7 μm) helped to explain why the two-layer electrode (4.89 μm thick) showed the most consistent efficiencies across all conditions. Complementarily, transient absorption spectroscopy was used to correlate the thicknesses with charge carrier lifetimes. Electron transfer to FTO was apparent only for the thinner electrode. Our work shows that the optimization of photoelectrocatalytic processes should include the number of layers as a key variable.

1. Introduction

Fujishima and Honda described in 1972 the photoelectrochemical splitting of water over TiO_2 electrodes.[1] Since then, many studies have investigated the photocatalytic properties of TiO_2, not only in powdered form[2–4] but also as single crystals[5–9] and films.[10–12] The application of such materials goes beyond photocatalysis, finding use as gas sensors, in solar cells, or as biomedical coatings.[13,14]

For photoelectrochemical applications, it is necessary to prepare films from TiO_2 powders, for which different methods exist, such as spin-coating,[15] dip-coating,[10] inkjet printing,[16] or growth over seeded substrates.[17] Even if the parent material is the same, the chosen method will considerably impact the photoactivity of the resulting films.[18] A particularly useful procedure is the screen-printing technique,[19] since it is fast, reproducible, and inexpensive, which makes it ideal for large-scale fabrication.[20,21] For this method a paste is prepared out of the photocatalyst powder and deposited through the mesh of a screen on an adequate substrate, and after a calcination step the electrode is obtained. The method has been widely applied for the preparation of electrodes for dye-sensitized solar cells (DSSCs).[22–24] One topic investigated within the research of DSSCs is the effect of the number of screen-printed layers on the efficiency of the devices. In general, two different behaviors are reported for the efficiencies of DSSCs as a function of the number of layers. Zhao *et al.*[25] and Ito *et al.*[22] showed a strong increase of the overall conversion efficiency from one to two layers, but a further increase of the number of layers did not significantly increase the conversion efficiency. Xie *et al.*[26] reported as well comparable conversion efficiencies for screen-printed TiO_2 electrodes with three to seven layers. On the other hand, a maximum for the conversion efficiency was reported by Zhang *et al.*[27] and Domtau *et al.*,[28] who found the optimal number of layers to be eight and three, respectively. Thus, either the efficiency raises by increasing the number of layers until a saturation level is reached,[22,25] or there is an optimal number of layers after which the efficiency decreases.[27,28] In these examples, nonetheless, there is no clear consensus on the physical reasons behind such behaviors.

Concerning the photoelectrochemical activity of bare TiO_2 electrodes, however, there are only a few reports investigating the effect of the number of screen-printed layers. For instance, Gimenez *et al.*[29] observed for screen-printed electrodes with

[a] C. Günnemann, Dr. M. Curti, J. Gerrit Eckert, Prof. Dr. D. W. Bahnemann
Institut für Technische Chemie
Gottfried Wilhelm Leibniz Universität Hannover
Hannover 30167 (Germany)
E-mail: guennemann@iftc.uni-hannover.de
curti@iftc.uni-hannover.de
[b] Dr. J. Schneider
Department of Chemistry
University of North Carolina at Chapel Hill
Chapel Hill NC-27599 (USA)
[c] Prof. Dr. D. W. Bahnemann
Laboratory "Photoactive Nanocomposite Materials"
Saint-Petersburg State University
Saint Petersburg 198504 (Russia)

Supporting information for this article is available on the WWW under https://doi.org/10.1002/cctc.201901872

This manuscript is part of the Special Issue "Photocatalysis: From Solar Power to Sustainable Chemical Production", which is part of the wider project "Building A New Energy Economy with Catalysis".

three different thicknesses (2.5 μm, 5 μm and 10 μm) that the most active ones for the water oxidation reaction are the 2.5 μm and 10 μm electrodes. Further, it was reported that the charge transfer occurs through TiO_2 (and not the substrate) only if the film is thick enough. These studies show that the number of layers is not only an important variable in order to maximize the photoelectrochemical efficiencies, but also represents an interesting tool to understand the underlying physical phenomena.

In this work, we investigated screen-printed TiO_2 electrodes with one, two, three, and four layers, and utilized them for the photoelectrochemical oxidation of methanol under different irradiation conditions and applied biases. The thickness-dependent behaviors can be explained on the basis of a diffusional model for electrons. Furthermore, as part of an extensive characterization, we analyzed the charge carrier kinetics by means of transient absorption spectroscopy in diffuse reflectance mode and modelled the decays with a second-order kinetic model.

Experimental Section

Chemicals

Hombikat UV100 TiO_2 (Sachtleben Chemie GmbH), acetic acid (100%, Carl Roth), ethanol (≥ 99.8%, Carl Roth), ethylcellulose (pure, Carl Roth), terpineol (pure, Carl Roth), acetylacetone (≥ 98%, Carl Roth), ammonium acetate (≥ 96%, Carl Roth), potassium hydroxide (1 N solution, Carl Roth), and methanol (≥ 99.9%, Carl Roth) were used as received without further purification.

Preparation of the Electrodes

Screen-printed TiO_2 electrodes were prepared using a modified version of the protocol described by Ito *et al.*[22] The detailed steps for the preparation of the paste for the screen-printing process are described in the Supporting Information. Fluorine-doped tin oxide (FTO, Sigma Aldrich) coated glass slides were used as substrates, for which they were cleaned in an ultrasonic bath, first with water and detergent and next with a mixture of acetone and water. The prepared paste was deposited on the substrates with a doctor blade through the mesh of a circle-shaped screen. Afterwards the coated slides were transferred to a heating plate and heated at 115 °C for several minutes for drying. To obtain multilayer electrodes subsequent coatings were applied after drying and cooling the slides to room temperature. Following the described process, the substrates were coated with one, two, three, or four layers of the paste. All electrodes were calcined afterwards at 500 °C for 4 hours on a heating plate to remove the organic compounds.

Characterization

X-ray diffraction (XRD) measurements were performed in a Bruker D8 Advance (USA) device with a Cu Kα source. The UV-vis reflectance spectroscopy measurements were carried out with an Agilent Technologies Cary 5000 (USA) spectrophotometer equipped with an Agilent DRA 2500 integrating sphere. Atomic force microscopy (AFM) measurements were performed by means of a Nanosurf Easyscan 2 (Switzerland) device. All measurements were performed at ambient pressure and at room temperature.

Photoelectrochemical Measurements

The photoelectrochemical measurements were performed using a three-electrode system with the TiO_2 deposited on FTO as working electrode, an Ag/AgCl reference electrode, and a platinum counter electrode. All measurements were carried out with a Zahner (Germany) Zennium potentiostat and a Zahner PECC-2 cell at ambient pressure and room temperature. Two samples of each electrode were analyzed, and the average was calculated. The chopped light voltammetry (CLV) measurements were performed in an electrolyte solution containing 0.1 M KOH and 10 vol-% methanol in deionized water, with a LOT-QuantumDesign (Germany) solar simulator consisting of a 300 W Xe lamp with an AM 1.5G filter (irradiance: 678 $W m^{-2}$). During the measurements the chopping of the solar simulator was done with a frequency of 200 mHz. The currents were recorded in a potential range from −0.7 V_{NHE} to 1.0 V_{NHE} with a scan rate of 20 $mV s^{-1}$; all potentials in this work are referred to the Normal Hydrogen Electrode (NHE). Incident photon-to-current conversion efficiency (IPCE) measurements were carried out with a Zahner TLS03 tunable light-emitting diode (LED) light source. The electrodes were illuminated in the aforementioned electrolyte solution with different LEDs (327 nm, 338 nm, 370 nm, and 385 nm), under applied potentials of 0.5 V_{NHE} and 0.2 V_{NHE} and a frequency of 1 Hz. For the Mott-Schottky measurements an aqueous 0.1 M KOH electrolyte and a frequency of 100 Hz were used.

Quantification of the Formaldehyde Production

The Nash method[30] was used to quantify the amount of the formaldehyde produced from the oxidation of methanol. To this end 500 μl aliquots of the anolyte were mixed with 500 μl of the Nash reagent (2 M ammonium acetate, 0.05 M acetic acid, 0.02 M acetylacetone). After an overnight incubation, the yellow-colored diacetyldihydrolutidine (DDL) is formed, which can be quantified by means of fluorescence spectroscopy.[31] Its excitation with a wavelength of 405 nm leads to an emission feature with a maximum at 510 nm. Concentrations were determined by integrating the area under the emission peak after performing a calibration curve. The measurements were performed in a well plate (Nunclon Delta Surface, Thermo Fisher Scientific Inc., USA) sample holder in a Hitachi F-7000 (Japan) fluorescence spectrophotometer.

Transient Absorption Spectroscopy

The electrodes were placed in a borosilicate glass cell, with their coated side directed to the window. For removal of the air the cell was flushed with N_2 or a mixture of N_2 and methanol for 30 minutes. The flushed cell was placed in the diffuse reflectance unit of an Applied Photophysics LKS 80 Photolysis Spectrometer with a pulsed Nd:YAG Laser (Quantel, Brilliant). The samples were excited with a 355 nm pulse (6 ns, 5 mJ) by using the third harmonic of the laser. Further details of the setup are given in reference[32].

During the measurement the absorbance (*Abs*) is recorded as a function of time. Since the measurements are performed in diffuse reflectance mode the *Abs* values need to be converted to the change in reflectance (ΔJ) using Equation (1), where J_0 is the reflectance before and J is the reflectance after the laser excitation.

$$\Delta J = 1 - 10^{-Abs} = \frac{J_0 - J}{J_0} \quad (1)$$

The concentration of the transients follows a linear relation with the change in reflectance as long as the latter is lower than 10%.[33] The measurements were performed in the wavelength range from 400 to 630 nm in 10 nm steps, 50 shots were averaged, and the data points were reduced to 200.

2. Results

2.1. Characterization

By weighing the FTO slides before and after the screen-printing process we obtained the mass of deposited TiO_2 to be between 1.55 and 6.75 mg, depending on the number of layers (Table 1, Figure S1). Within experimental error, the mass of TiO_2 is directly proportional to the number of layers. By considering the radius of the circle-shaped screen (1.1 cm), we estimated as well the mass coverages. Additionally, we determined the thicknesses of the films *via* AFM measurements (Table 1). Similar to the deposited TiO_2 mass, the thickness is directly proportional to the number of layers (Figure S1), indicating that all films have a similar porosity and no structural collapse occurs upon printing subsequent layers.

To determine the crystalline properties of the screen-printed TiO_2 electrodes we characterized them *via* XRD measurements. As shown in Figure 1, independently from the number of deposited layers, all electrodes exhibit reflections exclusively from the anatase modification of TiO_2, together with reflections from the FTO coating of the substrates. The intensity of the anatase reflections increases with the number of screen-printed layers, with a simultaneous decrease in the intensity of the FTO ones. The excerpt of the XRD patterns from 47° to 54° (Figure 1) shows this behavior more clearly. The increase and decrease in the intensity of the anatase and FTO reflections is monotonous.

In Figure 2 the UV-vis reflectance and absorbance spectra are given for all electrodes. With an increasing number of layers there is a monotonous increase in the fraction of reflected light in the visible range. In addition, we determined the band gaps of the electrodes from the absorption spectra *via* Tauc plots; the resulting graphs for all electrodes are given in the Supporting Information (Figure S2). The obtained band gaps are 3.19 ± 0.04 eV, 3.16 ± 0.03 eV, 3.16 ± 0.01 eV, and 3.17 ± 0.02 eV for the one-, two-, three-, and four-layer electrodes, respectively. Thus, the band gap is the same for all electrodes within the experimental error and does not change by increasing the number of layers. The fraction of reflected light in the UV range, on the other hand, is similar for all electrodes, and close to zero. This is observed as well in the absorbance spectra, where the highest absorbance occurs in the UV range. The onset of the absorption is similar for the multilayer electrodes, but slightly shifted to shorter wavelengths for the one-layer electrode, as indicated in the inset of Figure 2.

The electrodes were further analyzed *via* AFM to investigate the effect of multilayer screen-printing on their surficial morphology, Figure 3. The multilayer electrodes show similar variations in their heights, while for the one-layer electrode the variations are smaller. The same trend appears by comparing the root mean square roughness of the surfaces, with values of 16 ± 3 nm, 65 ± 7 nm, 64 ± 4 nm, and 62 ± 6 nm for the electrodes with one, two, three, and four layers, respectively.

Table 1. Masses, mass coverages, and thicknesses of the electrodes with one, two, three, and four screen-printed layers.

Number of layers	Mass [mg]	Mass coverage [mg cm^{-2}]	Thickness [µm]
1	1.55 ± 0.15	0.408 ± 0.040	2.67 ± 0.35
2	3.45 ± 0.35	0.908 ± 0.092	4.89 ± 0.25
3	5.00 ± 0.20	1.305 ± 0.053	7.09 ± 0.56
4	6.75 ± 0.55	1.776 ± 0.145	9.92 ± 1.05

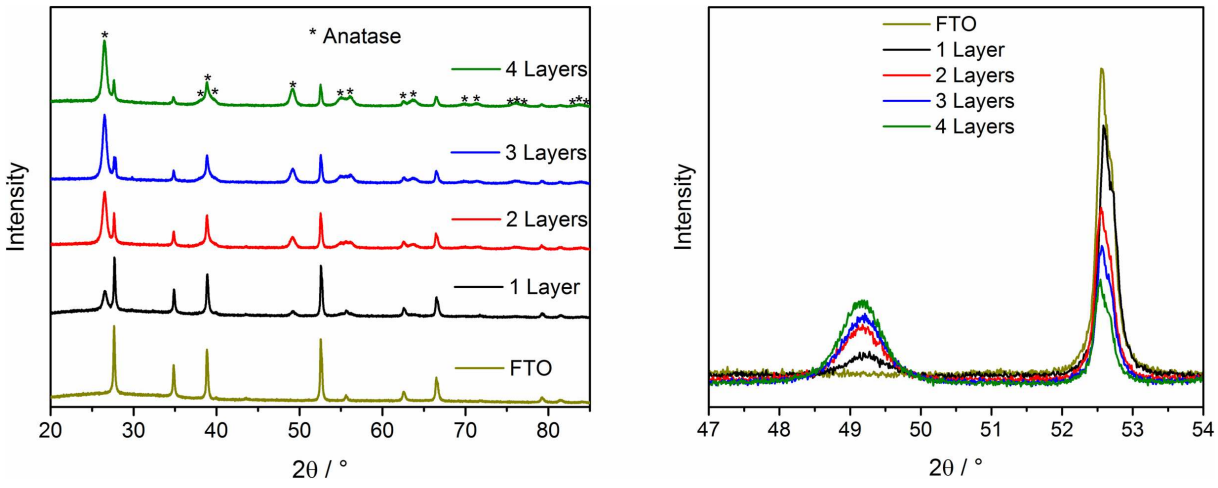

Figure 1. X-ray diffraction (XRD) pattern of the FTO substrate and of the electrodes with one, two, three and four layers (left) and excerpt of all XRD patterns in the range from 47° to 54° (right).

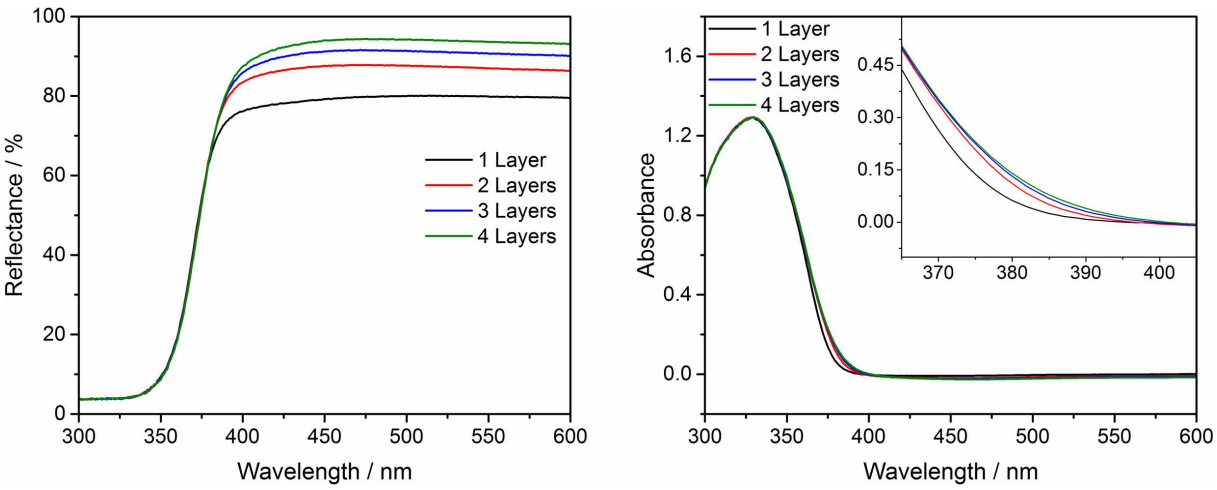

Figure 2. UV-vis reflectance spectra (left) and UV-vis absorbance spectra (right) of the screen-printed electrodes.

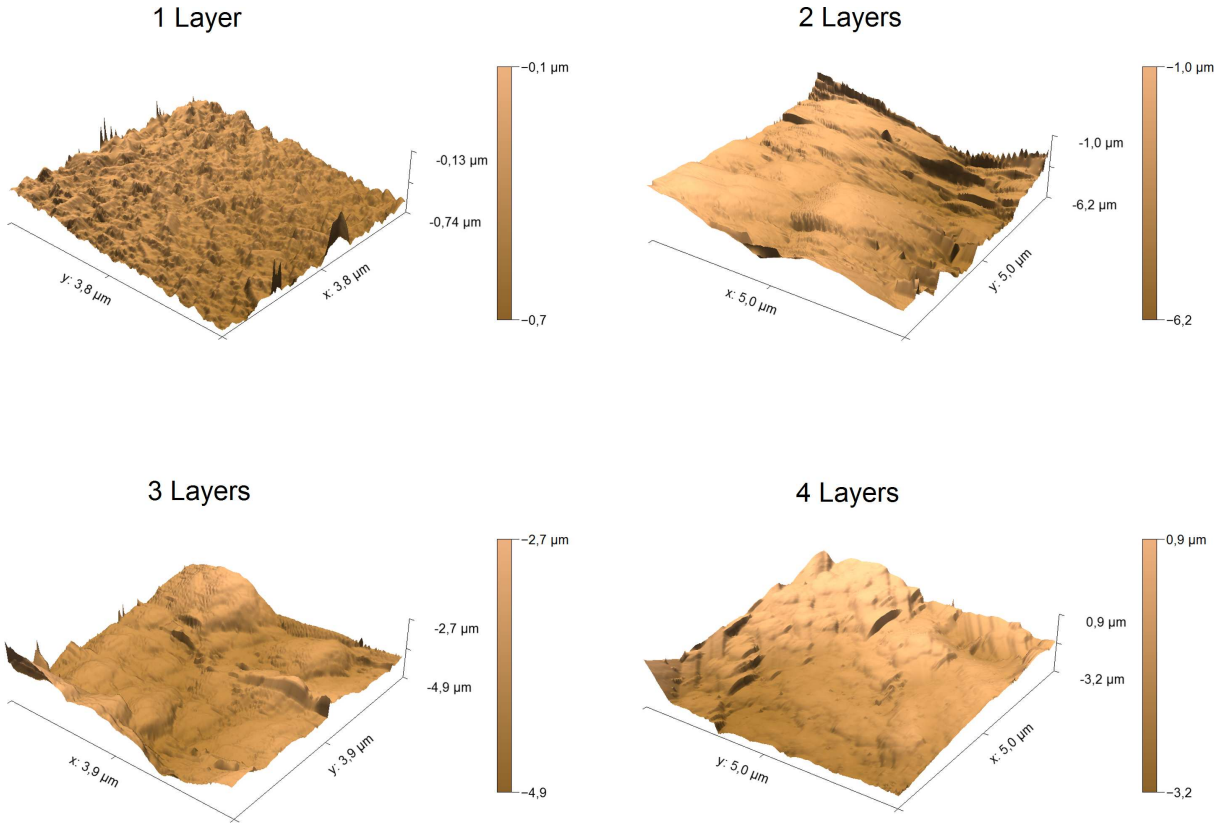

Figure 3. Atomic Force Microscopy (AFM) images of the electrodes with one (top left), two (top right), three (bottom left), and four (bottom right) layers.

2.2. Photoelectrochemical Methanol Oxidation

The flatband potentials of the electrodes (obtained from Mott-Schottky plots: capacitance^{-2} against applied potential) were measured in a 0.1 M KOH solution. For the electrodes with one to four printed layers the flatband potentials were quantified being $-0.71 \pm 0.14\ V_{NHE}$, $-0.80 \pm 0.06\ V_{NHE}$, $-0.81 \pm 0.04\ V_{NHE}$, and $-0.81 \pm 0.04\ V_{NHE}$, respectively. Considering the experimental error, the flatband potentials are similar for all electrodes.

The photoelectrochemical activity of the electrodes was analyzed *via* the oxidation of methanol in a basic electrolyte (0.1 M KOH and 10 vol-% methanol). Methanol is a typical model compound for the determination of the photocatalytic or photoelectrochemical activity of a material, since it is a small molecule, readily available, and colorless.[34] Furthermore, under

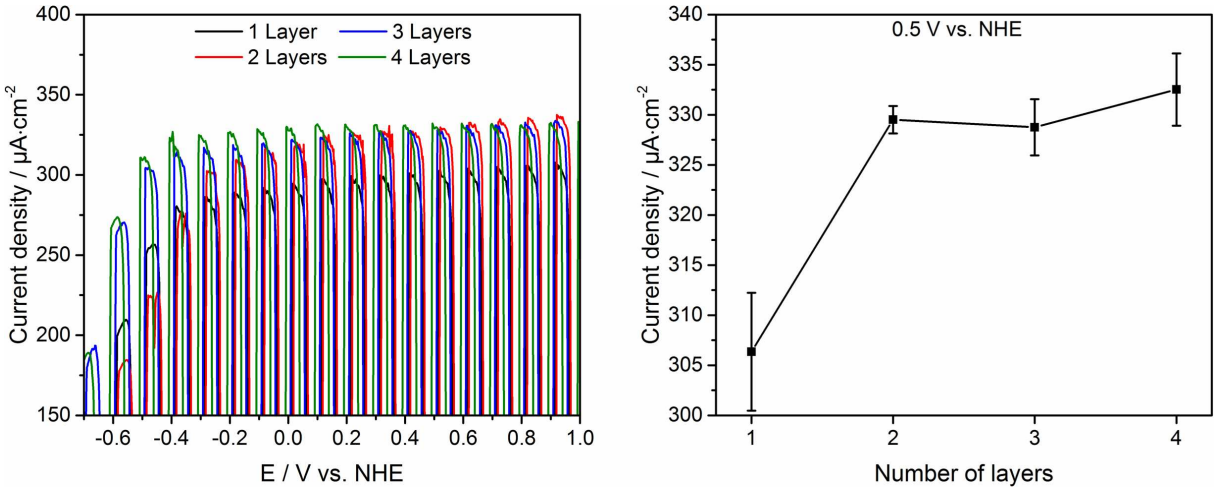

Figure 4. Chopped light voltammograms of all electrodes (left) and current densities at 0.5 V_{NHE} (right) in 0.1 M KOH with 10 vol-% methanol under irradiation with a solar simulator.

high methanol concentrations and low conversion fractions, the only stable oxidation product is formaldehyde, facilitating the analysis of the results.[34] Figure 4 shows the chopped light voltammograms (CLV) after irradiation with a solar simulator (i.e. a polychromatic source), while the Supporting Information displays all single voltammograms (Figure S3). All electrodes behave similarly: current densities under illumination increase when changing the bias from −0.6 V_{NHE} to −0.2 V_{NHE} and stay nearly constant for more positive potentials. On the other hand, at potentials more positive than ca. −0.3 V_{NHE} all multilayer electrodes show a higher current density than the electrode with one layer, with all of them showing similar current densities. This behavior is illustrated in Figure 4 at a potential of 0.5 V_{NHE}.

The dependence of the photocatalytic activity on the incident photon energy was tested utilizing monochromatic irradiation of different LEDs emitting at 327 nm, 338 nm, 370 nm, and 385 nm. The obtained IPCE values under a 0.5 V_{NHE} bias are shown in Figure 5. The overall shapes of the IPCE spectra agree with the absorption spectra of the films (cf. Figure 2); a larger absorbance translates to a higher utilization of the incident photons. At the shorter wavelengths the IPCE is inversely related with the number of layers, with the one-layer film being the most active, followed by the two-, three-, and four-layer electrodes. Upon moving to longer wavelengths, the trend reverses: for 385 nm irradiation the most active films are the thicker ones, and the one-layer film is the least active.

IPCE or photocurrent measurements are often used as the main benchmarks for the performance of photoelectrodes. However, depending on the intended application, the faradaic efficiency may actually be the most important parameter. In Figure 6 we show the measured photocurrents for the one-layer and four-layer electrodes under illumination with the solar simulator and the 338 nm LED. In all cases the photocurrent increases during the first minutes until reaching a steady state. Illumination with the solar simulator produces approximately

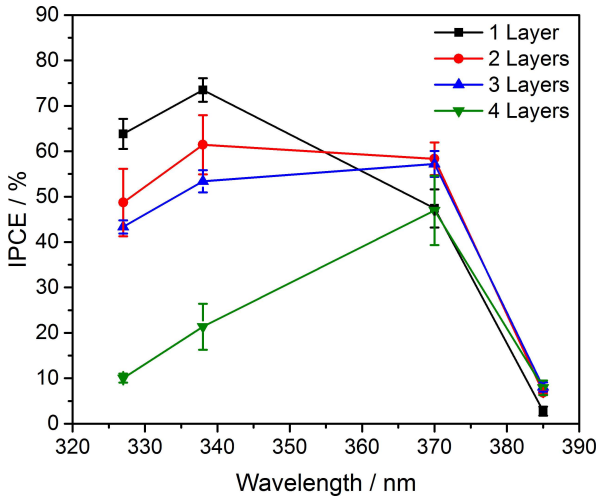

Figure 5. Incident photon-to-current efficiency (IPCE) values of the screen-printed electrodes at a potential of 0.5 V_{NHE} in a 0.1 M KOH with 10 vol-% methanol electrolyte.

three-fold higher currents than the 338 nm LED. Furthermore, the relative activity of the films changes: while the four-layer electrode is the most active under the solar simulator, the opposite is observed for 338 nm illumination. For the determination of the faradaic efficiencies we have quantified the amount of the main oxidation product, formaldehyde, after 10 minutes of irradiation. The faradaic efficiencies were 60±7 % and 56±6 % under the solar simulator irradiation, and 99±13% and 91±12% under illumination with the 338 nm LED, for the one- and four-layer electrodes, respectively. In both cases the differences between the electrodes are within experimental error. The irradiation source, on the other hand, has a sizeable effect: under LED irradiation the faradaic efficiency is close to unity, but for the solar simulator it is considerably lower.

Complementarily, to study the effect of the applied bias, we have performed IPCE measurements at a potential of 0.2 V_{NHE}. In

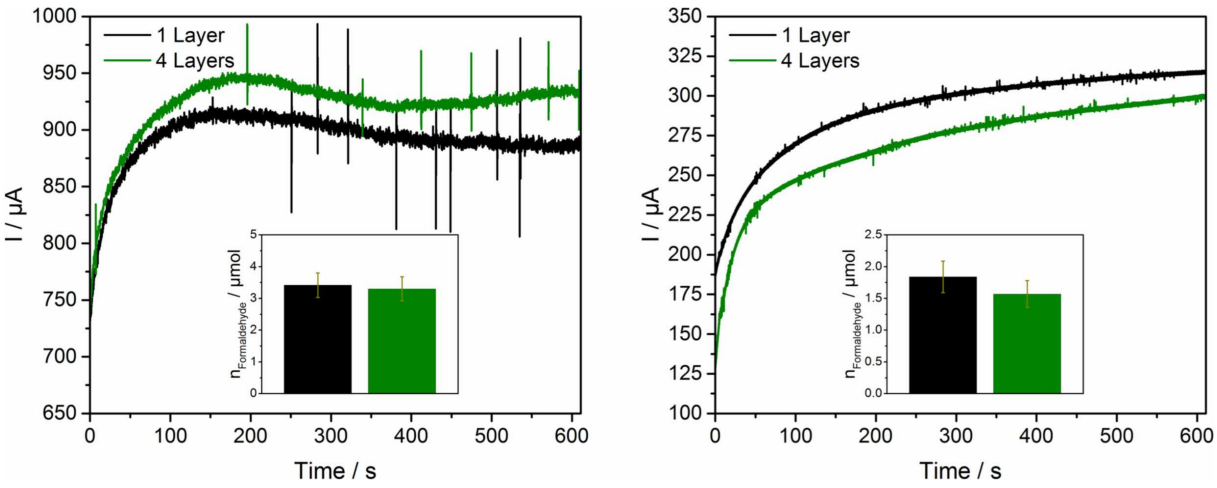

Figure 6. Photocurrent of the electrodes at 0.5 V_{NHE} in a 0.1 M KOH with 10 vol-% methanol electrolyte using the one-layer and four-layer electrodes under irradiation with the solar simulator (left) and the 338 nm LED (right). The insets show the detected amounts of formaldehyde after irradiation for 10 minutes.

Figure 7 the ratio between the IPCE values at 0.2 V_{NHE} and 0.5 V_{NHE} is given as a function of the excitation wavelength. The IPCE values are in all cases higher at a potential of 0.2 V_{NHE}, while the increase is most pronounced at the shorter wavelengths for the four-layer electrode. For the three-layer electrode the effect is smaller, but still a significant increase is observed at the shorter wavelengths. At the longer excitation wavelengths of 370 nm and 385 nm the 0.2 V_{NHE} potential increases the IPCE value for all electrodes in a similar ratio.

2.3. Transient Absorption Spectroscopy Measurements

In order to study the decay dynamics of the photogenerated charge carriers, we have performed transient absorption spectroscopy measurements in N_2 atmosphere and in a N_2 / methanol mixture for all the electrodes in the absence of applied bias. Figure 8 shows the transient absorption spectra of all electrodes 300 ns after their excitation with a 355 nm laser under N_2 atmosphere. All multilayer electrodes show a similar change in reflectance, ΔJ, and larger than that of the one-layer electrode. Since ΔJ is directly proportional to the number of photogenerated charge carriers, this shows that 300 ns after the pulse a smaller number of charge carriers survive in the one-layer electrode. The transient spectra for TiO_2 have reportedly two main components: one ascribed to trapped holes with a maximum at ~430 nm, and another broad signal with a maximum at ~650 nm corresponding to trapped electrons.[35]

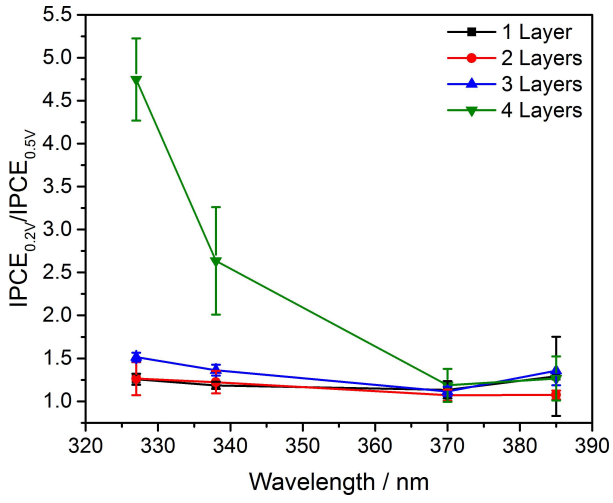

Figure 7. Ratio of the IPCE values obtained at the potentials 0.2 V_{NHE} and 0.5 V_{NHE}, at the excitation wavelengths 327 nm, 338 nm, 370 nm, and 385 nm for the electrodes with one, two, three, and four layers.

The transient absorption spectra of all electrodes in a N_2 / methanol mixture are given in Figure S4. A somewhat different situation arises: 300 ns after the excitation the highest number of charge carriers corresponds to the two-layer electrode, while the three- and four-layer electrodes show slightly lower signals, and the one-layer electrode shows again the lowest values. A similar picture is observed 5 µs after the excitation, although the differences between the multilayer electrodes are smaller. Additionally, the presence of methanol, a hole scavenger, alters the time evolution of the spectra: while an absorption band at around 400 nm assigned to holes[35] eventually disappears, a broad signal with a maximum at 620 nm related to electrons[35] slowly increases with time for all electrodes.

For the analysis of the decay kinetics we employed a second-order kinetic model as given in Equation (2), where A is related to the initial height of the signal, k is the decay rate constant, t the time, and B the baseline.[36,37]

$$\Delta J(t) = \frac{A}{A \cdot k \cdot t + 1} + B \quad (2)$$

We show the decay curves for the one-layer and four-layer electrodes under N_2 at a wavelength 600 nm, and their fits with Equation (2), in Figure 8 (the curves are virtually identical for all multilayer electrodes). The second-order kinetics describe very

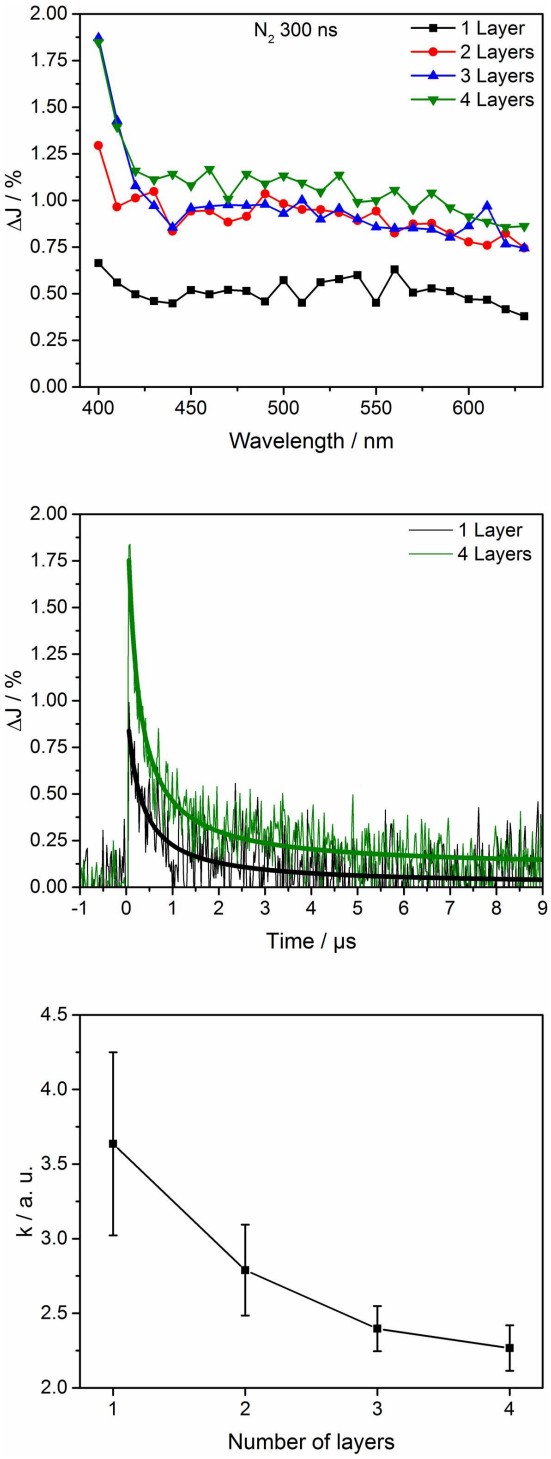

Figure 8. Transient absorption spectra 300 ns after the excitation with a 355 nm laser in N_2 atmosphere (top), decays at 600 nm of the electrodes with one and four layers (middle), and decay constants of all electrodes at 600 nm (bottom).

well the observed decays. In agreement with the transient spectra, all multilayer electrodes show overall higher signals than the one-layer one. From the fitting of the decays, we plot the obtained decay constants for all electrodes in Figure 8, as well. While the multilayer electrodes show similar values for the individual decay constants, the one-layer electrode shows a considerably larger decay constant at 600 nm.

3. Discussion

3.1. Characterization

The XRD patterns (Figure 1) reveal that after the calcination process at 500 °C all TiO_2 electrodes are in the anatase modification. This is in agreement with previous reports showing that UV100 TiO_2 particles do not transform to the rutile modification after heating below 600 °C.[38] Furthermore, the width of each reflection is homogeneous across all films, indicating that the crystalline properties are not affected by printing multiple layers.

Multilayer electrodes lead to thicker films, following a linear relationship with the number of layers: for each layer, the film thickness increases by about 2.5 ± 0.1 μm. This behavior impacts in different properties. For instance, an increase in the number of layers leads to higher intensities of the anatase XRD reflections concomitantly with a decrease in the intensities of the FTO reflections. Similarly, the deposited masses increase linearly with the number of layers, confirming the suitability of the method to prepare electrodes with controlled thicknesses. The different thicknesses are also apparent in the UV-vis reflectance measurements (Figure 2), where an increasing number of layers leads to an increased reflectance in the visible region. Interestingly, as evidenced in the absorption spectra, the absorption onset for the one-layer electrode is slightly shifted to shorter wavelengths compared to the multilayer electrodes. Since the crystallite sizes and film thicknesses are too large for the films to display quantum confinement effects,[39] a possible explanation is that the lower mass coverage and thickness of the one-layer electrode may yield slightly different optical properties. This would agree with the results from the AFM measurements (Figure 3), where higher surface roughnesses are observed for the multilayer electrodes compared to the one-layer one. On the other hand, although differences in porosity and surface roughness are indeed expected to affect the response of the electrodes,[16] the variations observed here are too small to exert a significant effect.

3.2. Photoelectrochemical Activity

The flatband potential measurements show similar values for all electrodes. Additionally, they agree well with previously reported values for the conduction band of TiO_2 particles, of ca. -0.75 V_{NHE} at pH 12.[40] Thus, for all electrodes it can be assumed that the flatband potential (E_{FB}) corresponds to the conduction band edge (E_{CB}), as can be expected for (highly doped) n-type semiconductors.[41] By combining the flatband potentials with the calculated bandgaps of Figure S1 we determined the positions of the valence bands (E_{VB}) for all electrodes, and sum up all values in Table S1. Since all electrodes show similar

flatband potentials and bandgaps, the valence band edges are similar as well. In Scheme 1 the values for the two-layer electrode are displayed as a representative example, together with the potentials of the water oxidation and reduction reactions, and the potentials of the methanol oxidation reaction. From this point of view all electrodes are able to oxidize methanol upon excitation; the water oxidation reaction, although thermodynamically more favorable, is not observed due to a high overpotential for oxygen evolution.[42]

We have performed the photoelectrochemical measurements in a 0.1 M KOH electrolyte with the addition of 10 vol-% methanol. To obtain a general idea of the ability of the electrodes to generate currents from its photoelectrochemical oxidation we performed CLV measurements under polychromatic irradiation (Figure 4). Although there are some variations at low biases, the behavior of all multilayer electrodes tends to equalize at higher applied potentials, while the one-layer electrode results in lower currents independently from the bias. This agrees well with the results of Fàbrega *et al.*,[45] who showed a similar photocurrent for WO_3 electrodes with thicknesses of 17.6, 11.5, and 8.1 μm at higher potentials, while the current of a thinner electrode (3.4 μm) was lower throughout. Further, Zhao *et al.*[25] and Ito *et al.*[22] reported for DSSCs with screen-printed TiO_2 electrodes a strong increase in the conversion efficiency from one to two layers, while for a higher number of layers the efficiency increased just slightly or stayed constant. Xie *et al.*[26] reported as well for DSSCs comparable conversion efficiencies for screen-printed TiO_2 electrodes with three to seven layers.

We observe a different trend for monochromatic illumination of the electrodes. The excitation with shorter wavelengths (327 nm and 338 nm) leads to IPCE values that decrease with an increasing number of layers. On the other hand, the excitation with 385 nm leads to increasing IPCEs as the number of layers increases. To explain this behavior two main factors must be analyzed. In the first place, a higher absorption coefficient will generally lead to a higher IPCE due to a better utilization of the incoming photons, as illustrated by the similar shapes of the absorbance and IPCE spectra. At a wavelength of 385 nm, and to a lesser extent at 370 nm, where the absorption coefficients of anatase TiO_2 are relatively small ($\alpha = 0.082\ \mu m^{-1}$ and $0.363\ \mu m^{-1}$, respectively[46]), light absorption increases with the number of layers, and consequently the IPCE benefits from a thicker film.

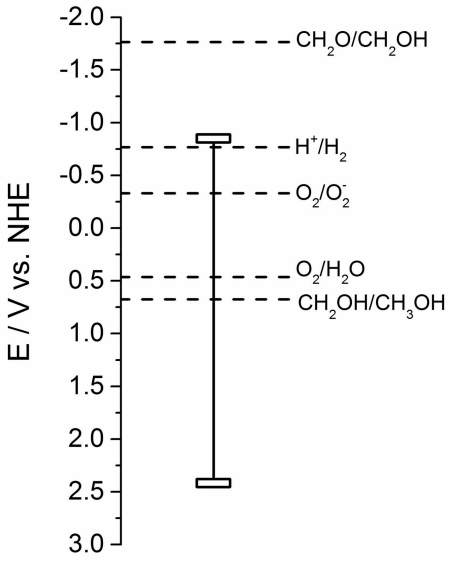

Scheme 1. Conduction band edge and valence band edge positions of the two-layer electrode with the relevant potentials for the methanol and water oxidation reactions, and for proton and oxygen reduction.[43,44] All values correspond to pH 13.

On the other hand, although they display very different IPCEs, all electrodes show a similar absorbance at wavelengths of 327 nm ($\alpha = 12.955\ \mu m^{-1}$)[46] and 338 nm ($\alpha = 6.487\ \mu m^{-1}$),[46] indicating the influence of a second factor. We note that, in photoelectrochemical reactions performed under frontside illumination, charge carriers are formed close to the electrode surface in contact with the electrolyte; under anodic bias, photogenerated electrons must diffuse through the entire film to reach the conductive FTO surface. Since the collection of photogenerated electrons by the external circuit is in direct competition with electron – hole recombination, longer diffusion distances will lead to lower IPCEs due to an increased rate of the latter.

Lindquist *et al.* have derived a theoretical model for microporous semiconductor films in photoelectrochemical cells under the assumption of diffusional charge carrier transport.[47] Of relevance for the present results, the model offers an expression for the IPCE under frontside illumination as a function of only three parameters: the absorption coefficient α, the film thickness d, and the average diffusion length of electrons before recombination L, Equation (3).

$$IPCE = \frac{\left[L\alpha\cosh\left(\frac{d}{L}\right) + \sinh\left(\frac{d}{L}\right) - L\alpha\, e^{d\alpha}\right] L\alpha\, e^{-d\alpha}}{\left[1 - L^2\alpha^2\right]\cosh\left(\frac{d}{L}\right)} \quad (3)$$

We now evaluate the IPCE results under this framework. To simplify the discussion, we focus on the relative IPCEs (i.e. the IPCE at each wavelength divided by the IPCE of the best performing electrode at that wavelength), Figure 9. By fitting this data to Equation 3 through a least-squares procedure we find that the model yields a very good description, which is notable since we employ only two adjustable parameters: L, and a scaling factor applied to the absorption coefficients from reference[46]. The latter is necessary since the reported α values correspond to a dense film, contrarily to the present mesoporous electrodes. As a result of the fitting we obtain a scaling factor of 0.48, in very good agreement with the estimated average density of our films (1.75 $g\,cm^{-3}$, i.e. 46% that of bulk anatase).

From the qualitative point of view, the model reproduces the behavior of all electrodes, with the only exception found at the short-wavelength side, where it predicts, contrary to our observations, wavelength-independent efficiencies. The discrepancy is higher as the film thickness increases, suggesting that

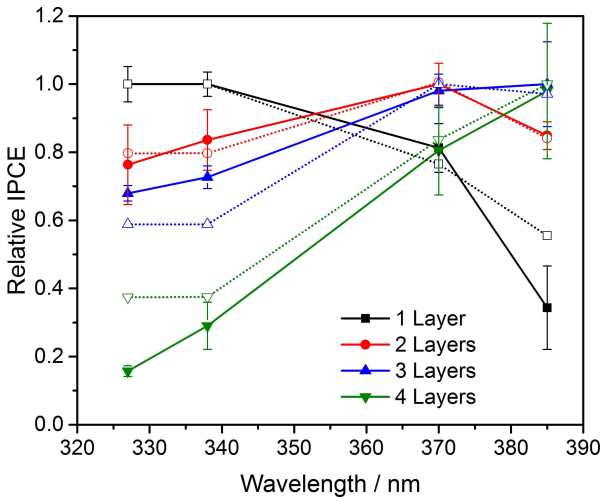

Figure 9. Relative incident photon-to-current efficiency (IPCE) values calculated with respect to the best performing electrode at each wavelength (solid symbols). Hollow symbols show the values calculated from the diffusional model of Lindquist et al.,[47] from where we obtain a diffusion length for electrons of 5.7 μm. The experimental data corresponds to an applied potential of 0.5 V_{NHE} and a 0.1 M KOH with 10 vol-% methanol electrolyte. Solid and dotted lines connect the experimental and calculated data points, respectively, as guides for the eye.

the assumptions from the model[47] are best fulfilled in the thinner films.

Additionally, we estimate the electron diffusion length to be $L = 5.7$ μm. This value is comparable to that reported by Leng *et al.*, between 8.5 μm and 12.5 μm for mesoporous TiO_2 electrodes in a water splitting system at pH 2, independently from the applied bias.[48] The application of the model shows that, as expected for frontside illumination, film thicknesses above the diffusion length are very detrimental for the efficiencies, especially considering that a thickness of ca. 5.7 μm is enough to completely absorb light in a broad spectral range. Indeed, the two-layer film, with a thickness of 4.89 μm, shows the most consistent efficiencies across all wavelengths (Figure 9).

When applied to the absolute IPCE results (and not to the relative values) the model does not correctly predict their magnitude (Figure S5). However, it does describe very satisfactorily the thickness dependence of the IPCE, even while many of the assumptions[47] on which the model is based may not be valid for the present system.

Importantly, these results indicate that the thickness must be carefully chosen to strike the balance between two factors: while thicker films ensure complete light absorption, the average distance of the photogenerated electrons to the back contact may be too large to achieve enough charge separation as to prevent significant recombination. At wavelengths where the absorption coefficient is small, in accordance to Lambert – Beer's law, charge carriers are photogenerated across the entire film, diffusion times are relatively short, and thicker films show the best IPCEs because they absorb larger fractions of light. Contrarily, when the absorption coefficient is large, all light will be absorbed within the first layers of the electrodes; in this case, it is beneficial to have a thinner film, in order to diminish the diffusion time to the back contact (Scheme 2). The two-layer film, with a thickness slightly below the diffusion length, offers the overall best activity due to a good balance between these factors.

Since our objective in this work is not only to optimize the number of screen-printed layers but also to gain insights on the underlying physical processes, we have also measured the IPCEs at a potential of 0.2 V_{NHE} (Figure 7). Interestingly, although this value is less anodic than the 0.5 V_{NHE} employed for the remaining experiments, all electrodes yield higher IPCEs under

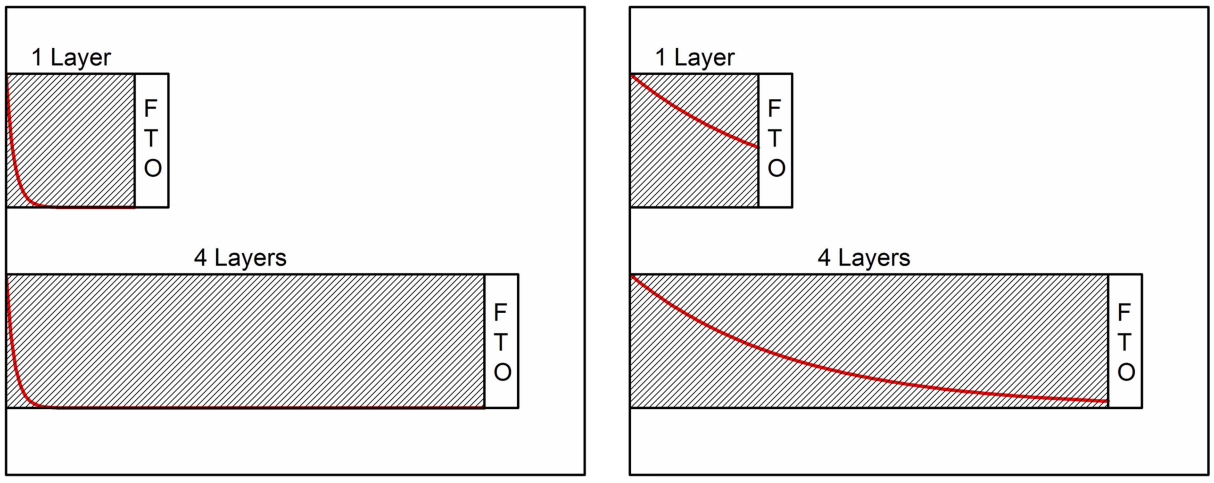

Scheme 2. Illustrations of the light absorption profiles (light intensity as a function of depth, red line) for the shorter wavelengths (327 nm and 338 nm, left) and the longer wavelengths (370 nm and 385 nm, right) for the one-layer electrode and the four-layer electrode under frontside irradiation. Since the penetration depth is rather shallow for the shorter wavelengths, both electrodes are thick enough to completely absorb the incoming light, and the electron-hole pairs are generated relatively far away from the FTO back contact. Contrarily, the penetration depth of the longer wavelengths is significantly higher, and thus only the four-layer electrode achieves complete absorption. Furthermore, on average, electron-hole pairs are generated relatively close to the back contact.

0.2 V_{NHE}, with a more pronounced effect at the shorter wavelengths and for the thicker electrodes. Since all electrodes absorb a similar fraction of light at these wavelengths (Figure 2), these results strongly suggest that the 0.5 V_{NHE} bias actually hinders the diffusion of electrons to the back contact in comparison with a 0.2 V_{NHE} bias. Indeed, by fitting the IPCE data at 0.2 V_{NHE} with Equation 3 we find a diffusion length of 9.1 μm, considerably longer than that at 0.5 V_{NHE} (5.7 μm). As recently shown for WO_3 photoanodes, a more anodic bias, by extracting electrons well below the conduction band edge (Scheme 1), may empty a larger range of intra-bandgap (trap) states. Therefore, in their way to the back contact, photogenerated electrons will experiment repeated trapping-detrapping steps, effectively decreasing their diffusion length and reducing the IPCE.[49] As discussed above, the very shallow penetration depths of the shorter wavelengths is more detrimental for the thicker films; at 0.5 V_{NHE}, the decrease in the diffusion coefficient caused by trap emptying exacerbates this problem.

Since the intended application of photoelectrocatalysis most likely involves (polychromatic) sunlight as the excitation source, it is also important to consider such conditions. We find here that under simulated solar light all multilayer electrodes show a similar activity, higher with respect to the one-layer electrode. To explain this behavior, we refer to the contribution of each wavelength to the solar spectrum. As discussed above, the IPCEs show two distinct behaviors: one at short wavelengths and another at the longer ones; the middle point is at around 354 nm. In the 300–354 nm spectral region, the irradiance of the employed solar simulator (Figure S6) is 6.5 $W m^{-2}$, while for the 354 to 395 nm range it is 11 $W m^{-2}$. Therefore, the behavior under polychromatic irradiation is more similar to that under the longer monochromatic wavelengths, where the low thickness of the one-layer electrode means a considerable fraction of light transmits through them, decreasing the IPCE (Scheme 2).

To facilitate the comparison with previous reports we have so far centered our discussion on photogenerated currents and IPCEs derived from them. Nonetheless, the performance assessment of a photoelectrochemical device should also include the faradaic efficiencies. We have selected here four representative cases: irradiation either with the solar simulator or with a monochromatic (338 nm) LED, and either one-layer or four-layer films, for which we measured the methanol oxidation photocurrent under a bias of 0.5 V_{NHE} during 10 minutes, and afterwards determined the amount of formaldehyde in solution. In terms of the photocurrent, we obtain results consistent with the former observations by varying the film thickness or irradiation source (Figure 6). The faradaic efficiencies, on the other hand, are different: while for the monochromatic illumination they are virtually unitary (99 ± 13% and 91 ± 12% for the one- and four-layer electrodes), under the solar simulator the faradaic efficiencies only reach 60 ± 7% (one layer) and 56 ± 6% (four layers). As reference values, we note that Wahl *et al.*[50] reported a faradaic efficiency of 30% for the oxidation of methanol over rutile electrodes, while Mesa *et al.*[51] showed a faradic efficiency of 96% for the same reaction over hematite electrodes. To rationalize our results we observe that, as illustrated by the ca. three-fold higher photocurrents, the intensity of the solar simulator is considerably higher than that of the LED. In addition, although at low formaldehyde concentrations the oxidation of methanol is overwhelmingly favored, the accumulation of the former gradually brings its own oxidation to compete with that of methanol, aided by a rate constant for hole scavenging that is double as high for formaldehyde than for methanol[52] and by the fact that each molecule of produced formaldehyde must desorb from the surface for another methanol molecule to be oxidized.[53] Consequently, as the reaction progresses (or light intensity increases), more formaldehyde will be oxidized to formic acid, lowering the faradaic efficiency for the formaldehyde production. As an example, for the gas-phase photocatalytic methanol oxidation reaction it has been shown that, at low molar fractions of methanol in relation to water, the main products are CO_2, formaldehyde, and formic acid.[54] Thus, a lower detected amount of formaldehyde is associated to higher produced amounts of formic acid and/or CO_2.

3.3. Charge Carrier Kinetics

We studied the charge carrier kinetics upon exciting the electrodes both under inert (N_2) and reactive (N_2/methanol) atmospheres, by means of transient absorption spectroscopy. At the excitation wavelength, 355 nm, the multilayer electrodes absorb only slightly more light than the one-layer electrode (Figure 2), in agreement with the penetration depth associated with the reported absorption coefficient ($\alpha = 1.6579\ \mu m^{-1}$).[46] From this information we infer that the number of charge carriers generated from the laser pulse is approximately equal for all electrodes. The transient spectra taken at early times under inert or reactive atmospheres, however, show a significantly lower signal for the one-layer electrode (Figure 8, Figure S4). We note that 300 ns after the pulse represents a relatively long time for the ultrafast recombination processes,[55] and thus the observed initial signal most likely does not represent the number of photogenerated charge carriers but rather the number of those which survived recombination. As shown in Figure 8, the decay constant for electrons is approximately 60% faster for the one-layer electrode than for the four-layer one. Assuming that the kinetics are transferrable to the sub-μs time range, the faster decay of the electron's (broad) transient absorption explains why the spectra of the one-layer electrode shows overall lower signals. Regarding the reason for the faster electron decay in this electrode, we recall the observations of Levy *et al*,[56] who reported that backside (but not frontside) illumination of an 8 μm thick TiO_2 film on FTO with a short wavelength (337 nm) causes a flow of photogenerated electrons to the back contact even in the absence of an applied bias. This suggests that, as long as electrons are photogenerated close to the FTO, an efficient flow can occur, accelerating their disappearance rate as observed by transient absorption spectroscopy. Importantly, since the one-layer electrode is considerably thinner than that of Levy *et al.* (2.67 μm vs 8 μm), and the excitation wavelength has a higher

penetration depth, we are able to observe such electron transfer for frontside illumination, although not for the (thicker) multilayer electrodes.

In summary, the transient absorption spectroscopy results support the conclusions from the photoelectrochemical experiments: even in the absence of applied bias, photogenerated electrons diffuse towards the back contact, decreasing the recombination rate. However, there is a delicate interplay between light's penetration depth and electrode thickness: if the latter is too large with respect to the former, the photogenerated electrons will not benefit from the charge separation offered by the back contact sink, and thus the most likely fate of charge carriers will be recombination.

4. Conclusions

We analyzed the photoelectrochemical behavior of anatase TiO_2 electrodes deposited on FTO-coated glass by the versatile and easily scalable screen-printing technique. Our focus was on optimizing the number of printed layers to maximize the photoinduced oxidation of methanol under anodic bias and frontside illumination. We found that the number of layers, directly proportional to the film thickness, has varying effects on the incident photon-to-current efficiency (IPCE) depending on the applied bias and the irradiation wavelength. Regarding the former, we found that, contrary to expectations, more anodic biases may be detrimental due to a trap emptying effect that rises electron diffusion time to the back electrode; this effect is more pronounced as the film thickness increases. With respect to the irradiation wavelength, we found two opposing factors: while for longer wavelengths (where absorption coefficients are small) the IPCE benefits from thicker films, at the shorter wavelengths (where complete absorption occurs far from the back contact) the thinner films show much higher efficiencies. Additionally, we modelled our results with a previously proposed diffusional model for electrons, which quantitatively confirms the necessity to balance these factors. Under simulated solar light the observed behavior is a convolution between these effects and the emission spectrum of the excitation source, which emphasizes the influence of the longer wavelengths. Our observations are supported by transient absorption spectroscopy measurements that show that electron transfer to FTO can occur even without applied bias, although only if the film is thin enough for diffusion to significantly occur.

All in all, the two-layer electrode, with a thickness of 4.89 μm, yields a good balance between all factors: it is thick enough to ensure nearly complete light absorption under most conditions, but thin enough to ensure a good electron collection from the back electrode.

Acknowledgements

The authors thank Dipl.-Chem. Verena Becker for performing the AFM measurements. CG and JS acknowledge financial support from the Leibniz Universität Hannover within the program "Wege in die Forschung II". MC is grateful to the Deutscher Akademischer Austauschdienst (DAAD) together with the Ministerio de Educación, Cultura, Ciencia y Tecnología (Argentina) for his ALEARG scholarship. This work was supported by Saint-Petersburg State University via a research Grant ID 32706707.

Conflict of Interest

The authors declare no conflict of interest.

Keywords: Photocatalysis · Photoelectrocatalysis · Solar energy conversion · Photoelectrochemistry · Titanium dioxide

[1] A. Fujishima, K. Honda, *Nature* **1972**, *238*, 37–38.
[2] A. Mattsson, L. Österlund, *J. Phys. Chem. C* **2010**, *114*, 14121–14132.
[3] K. Okamoto, Y. Yamamoto, H. Tanaka, M. Tanaka, A. Itaya, *Bull. Chem. Soc. Jpn.* **1985**, *58*, 2015–2022.
[4] W. Xu, D. Raftery, *J. Phys. Chem. B* **2001**, *105*, 4343–4349.
[5] A. Y. Ahmed, T. A. Kandiel, T. Oekermann, D. Bahnemann, *J. Phys. Chem. Lett.* **2011**, *2*, 2461–2465.
[6] L. Kavan, M. Grätzel, S. E. Gilbert, C. Klemenz, H. J. Scheel, *J. Am. Chem. Soc.* **1996**, *118*, 6716–6723.
[7] C. Haisch, C. Günnemann, S. Melchers, M. Fleisch, J. Schneider, A. V. Emeline, D. W. Bahnemann, *Electrochim. Acta* **2018**, *280*, 278–289.
[8] C. Günnemann, C. Haisch, M. Fleisch, J. Schneider, A. V. Emeline, D. W. Bahnemann, *ACS Catal.* **2019**, *9*, 1001–1012.
[9] T. Luttrell, S. Halpegamage, J. Tao, A. Kramer, E. Sutter, M. Batzill, *Sci. Rep.* **2014**, *4043*, 1–8.
[10] J. Freitag, D. W. Bahnemann, *ChemPhysChem* **2015**, *16*, 2670–2679.
[11] I. Sopyan, M. Watanabe, S. Murasawa, K. Hashimoto, A. Fujishima, *J. Photochem. Photobiol. A* **1996**, *98*, 79–86.
[12] K. Sunada, Y. Kikuchi, K. Hashimoto, A. Fujishima, *Environ. Sci. Technol.* **1998**, *32*, 726–728.
[13] D. Nunes, A. Pimentel, A. Gonçalves, S. Pereira, R. Branquinho, P. Barquinha, E. Fortunato, R. Martins, *Semicond. Sci. Technol.* **2019**, *34*, 043001.
[14] P. Roy, S. Berger, P. Schmuki, *Angew. Chem. Int. Ed.* **2011**, *50*, 2904–2939; *Angew. Chem.* **2011**, *123*, 2956–2995.
[15] G. Waldner, M. Pourmodjib, R. Bauer, M. Neumann-Spallart, *Chemosphere* **2003**, *50*, 989–998.
[16] I. Bernacka-Wojcik, P. J. Wojcik, H. Aguas, E. Fortunato, R. Martins, *J. Colloid Interface Sci.* **2016**, *465*, 208–214.
[17] D. Nunes, A. Pimentel, L. Santos, P. Barquinha, E. Fortunato, R. Martins, *Catalysts* **2017**, *7*, 60.
[18] G. Waldner, J. Krýsa, *Electrochim. Acta* **2005**, *50*, 4498–4504.
[19] C. Haisch, J. Schneider, M. Fleisch, H. Gutzmann, T. Klassen, D. W. Bahnemann, *Dalton Trans.* **2017**, *46*, 12811–12823.
[20] F. C. Krebs, M. Jørgensen, K. Norrman, O. Hagemann, J. Alstrup, T. D. Nielsen, J. Fyenbo, K. Larsen, J. Kristensen, *Sol. Energy Mater. Sol. Cells* **2009**, *93*, 422–441.
[21] S. E. Shaheen, R. Radspinner, N. Peyghambarian, G. E. Jabbour, *Appl. Phys. Lett.* **2001**, *79*, 2996–2998.
[22] S. Ito, P. Chen, P. Comte, M. K. Nazeeruddin, P. Liska, P. Péchy, M. Grätzel, *Prog. Photovolt: Res. Appl.* **2007**, *15*, 603–612.
[23] U. O. Krašovec, M. Berginc, M. Hočevar, M. Topič, *Sol. Energy Mater. Sol. Cells* **2009**, *93*, 379–381.
[24] H. Chang, Y. Yang, H. Li, C. Hsu, I. Cheng, J. Chen, *J. Power Sources* **2013**, *234*, 16–22.
[25] W. Zhao, H. Bala, J. Chen, Y. Zhao, G. Sun, J. Cao, Z. Zhang, *Electrochim. Acta* **2013**, *114*, 318–324.
[26] D. M. Xie, S. J. Feng, Y. Lin, G. J. Dong, X. R. Xiao, X. P. Li, X. W. Zhou, *Chinese Sci. Bull.* **2007**, *52*, 2481–2485.
[27] H. Zhang, W. Wang, H. Liu, R. Wang, Y. Chen, Z. Wang, *Mater. Res. Bull.* **2014**, *49*, 126–131.
[28] D. L. Domtau, J. Simiyu, E. O. Ayieta, L. O. Nyakiti, B. Muthoka, J. M. Mwabora, *Surf. Rev. Lett.* **2017**, *24*, 1750065.

[29] S. Gimenez, H. K. Dunn, P. Rodenas, F. Fabregat-Santiago, S. G. Miralles, E. M. Barea, R. Trevisan, A. Guerrero, J. Bisquert, *J. Electroanal. Chem.* **2012**, *668*, 119–125.
[30] T. Nash, *Biochem. J.* **1953**, *55*, 416–421.
[31] S. Belman, *Anal. Chim. Acta* **1963**, *29*, 120–126.
[32] A. Arimi, C. Günnemann, M. Curti, D. W. Bahnemann, *Catalysts* **2019**, *9*, 697.
[33] R. W. Kessler, G. Krabichler, S. Uhl, D. Oelkrug, W. P. Hagan, J. Hyslop, F. Wilkinson, *Opt. Acta* **1983**, *30*, 1099–1111.
[34] A. Y. Ahmed, T. A. Kandiel, I. Ivanova, D. Bahnemann, *Appl. Surf. Sci.* **2014**, *319*, 44–49.
[35] D. W. Bahnemann, M. Hilgendorff, R. Memming, *J. Phys. Chem. B* **1997**, *101*, 4265–4275.
[36] F. Sieland, J. Schneider, D. W. Bahnemann, *J. Phys. Chem. C* **2017**, *121*, 24282–24291.
[37] C. Günnemann, M. Curti, J. Schneider, D. W. Bahnemann, *Photochemistry, Vol. 47*, (Eds.: A. Albini, S. Protti), The Royal Society Of Chemistry, **2020**, pp. 122–158.
[38] M. A. Behnajady, M. E. Alamdari, N. Modirshahla, *Environ. Prot. Eng.* **2013**, *39*, 33–46.
[39] C. Kormann, D. W. Bahnemann, M. R. Hoffmann, *J. Phys. Chem.* **1988**, *92*, 5196–5201.
[40] K. Vinodgopal, S. Hotchandani, P. V. Kamat, *J. Phys. Chem.* **1993**, *97*, 9040–9044.
[41] D. E. Scaife, *Sol. Energy* **1980**, *25*, 41–54.
[42] J. Chen, Y. F. Li, P. Sit, A. Selloni, *J. Am. Chem. Soc.* **2013**, *135*, 18774–18777.
[43] Y. A. Ilan, G. Czapski, D. Meisel, *Biochim. Biophys. Acta* **1976**, *430*, 209–224.
[44] C. Wang, R. Pagel, D. W. Bahnemann, J. K. Dohrmann, *J. Phys. Chem. B* **2004**, *108*, 14082–14092.
[45] C. Fàbrega, S. Murcia-López, D. Monllor-Satoca, J. D. Prades, M. D. Hernández-Alonso, G. Penelas, J. R. Morante, T. Andreu, *Appl. Catal. B* **2016**, *189*, 133–140.
[46] T. Siefke, S. Kroker, K. Pfeiffer, O. Puffky, K. Dietrich, D. Franta, I. Ohlídal, A. Szeghalmi, E. B. Kley, A. Tünnermann, *Adv. Opt. Mater.* **2016**, *4*, 1780–1786.
[47] S. Södergren, A. Hagfeldt, J. Olsson, S.-E. Lindquist, *J. Phys. Chem.* **1994**, *98*, 5552–5556.
[48] W. H. Leng, P. R. F. Barnes, M. Juozapavicius, B. C. O'Regan, J. R. Durrant, *J. Phys. Chem. Lett.* **2010**, *1*, 967–972.
[49] S. Corby, L. Francàs, S. Selim, M. Sachs, C. Blackman, A. Kafizas, J. R. Durrant, *J. Am. Chem. Soc.* **2018**, *140*, 16168–16177.
[50] A. Wahl, M. Ulmann, A. Carroy, B. Jermann, M. Dolata, P. Kedzierzawski, C. Chatelain, A. Monnier, J. Augustynski, *J. Electroanal. Chem.* **1995**, *396*, 41–51.
[51] C. A. Mesa, A. Kafizas, L. Francàs, S. R. Pendlebury, E. Pastor, Y. Ma, F. Le Formal, M. T. Mayer, M. Grätzel, J. R. Durrant, *J. Am. Chem. Soc.* **2017**, *139*, 11537–11543.
[52] N. M. Dimitrijevic, I. A. Shkrob, D. J. Gosztola, T. Rajh, *J. Phys. Chem. C* **2012**, *116*, 878–885.
[53] G. L. Chiarello, D. Ferri, E. Selli, *J. Catal.* **2011**, *280*, 168–177.
[54] G. L. Chiarello, M. H. Aguirre, E. Selli, *J. Catal.* **2010**, *273*, 182–190.
[55] J. Schneider, M. Matsuoka, M. Takeuchi, J. Zhang, Y. Horiuchi, M. Anpo, D. W. Bahnemann, *Chem. Rev.* **2014**, *114*, 9919–9986.
[56] B. Levy, W. Liu, S. E. Gilbert, *J. Phys. Chem. B* **1997**, *101*, 1810–1816.

Manuscript received: October 2, 2019
Revised manuscript received: November 5, 2019
Accepted manuscript online: November 6, 2019
Version of record online: December 2, 2019